INTERNATIONAL JOURNAL FOR NUMERICAL METHODS IN FLUIDS
Int. J. Numer. Meth. Fluids 2008; **56**:1139–1145
Published online 19 September 2007 in Wiley InterScience (www.interscience.wiley.com). DOI: 10.1002/fld.1589

A multilevel domain decomposition approach to solving coupled applications in computational fluid dynamics

Eugenio Aulisa[1], Sandro Manservisi[1, 2, *, †] and Padmanabhan Seshaiyer[1]

[1]*Department of Mathematics and Statistics, Texas Tech University, Lubbock, TX 79409-1042, U.S.A.*
[2]*DIENCA, University of Bologna, via dei colli 16, 40134 Bologna, Italy*

SUMMARY

Direct numerical simulation of the non-linear equations, governing a fluid–structure system, relies heavily on the properties of the coupled system and the corresponding iterative solver. The purpose of this paper is to introduce a flexible and robust multilevel finite element algorithm that can be used to study the behavior of a fully coupled fluid–structure system. The method relies on the domain decomposition characteristics of the multigrid Vanka solvers, which decompose the complex global domain into the finite element local sub-domains and then compute the global solution iteratively. This particular methodology allows us to solve easily this coupled system over a fluid–solid domain which consists of a set of subdomains from different mesh levels with conforming or non-conforming finite element method approximations. The multigrid projection and restriction operators are used to impose the matching between the extended fluid and solid velocity field. Copyright © 2007 John Wiley & Sons, Ltd.

Received 2 April 2007; Revised 26 June 2007; Accepted 10 July 2007

KEY WORDS: fluid–structure interaction; multilevel domain decomposition; multigrid solver

1. INTRODUCTION

The direct numerical simulation of a fluid–structure system involves the coupled solution of the Navier–Stokes system and the structural mechanical equations. Let the computational domain $\Omega \subset \Re^2$ be the union of the fluid subdomain Ω_f, where the unsteady Navier–Stokes equations for incompressible flow are solved, and the solid subdomain Ω_s, where the linear elasticity equations are considered. Let us assume that any boundaries can change in time. In this regard, let the

*Correspondence to: Sandro Manservisi, DIENCA, University of Bologna, via dei colli 16, 40134 Bologna, Italy.
†E-mail: sandro.manservisi@mail.ing.unibo.it

Contract/grant sponsor: Computational Mathematics, National Science Foundation; contract/grant number: DMS 0610026
Contract/grant sponsor: Texas Higher Education Coordinating Board, Advanced Research Program; contract/grant number: ARP 0212-44c399

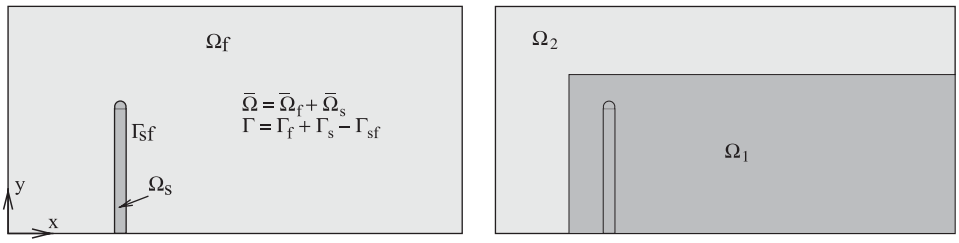

Figure 1. Domain decomposition of $\Omega = \Omega_f \cup \Omega_s$ in fluid and solid subdomains (on the left) and non-conforming decomposition $\Omega = \Omega_1 \cup \Omega_2$ (on the right).

subdomains Ω_f and Ω_s be time dependent and constrained by $\bar{\Omega}_f(t) \cup \bar{\Omega}_s(t) = \bar{\Omega}(t)$. Figure 1 on the left illustrates the computational domain Ω with fluid and solid boundary Γ_f and Γ_s, respectively. We denote the boundary of Ω by Γ and the interior boundary between Ω_f and Ω_s by Γ_{sf}.

The fluid velocity, the fluid pressure and the solid displacement $(\mathbf{u}, p, \mathbf{w}) \in \mathbf{H}^1(\Omega_f) \times L^2(\Omega_f) \times \mathbf{H}^1(\Omega_s)$ satisfy the weak variational form of the unsteady fully coupled fluid–structure problem given by

$$\int_{\Omega_f} \rho_f \left(\frac{\partial \mathbf{u}}{\partial t} + (\mathbf{u} \cdot \nabla)\mathbf{u} \right) \cdot \mathbf{v} \, d\mathbf{x} + \int_{\Omega_f} (2\mu_f D(\mathbf{u}) : D(\mathbf{v}) - p\nabla \cdot \mathbf{v}) \, d\mathbf{x} + \int_{\Gamma_{sf}} \boldsymbol{\lambda}_1 \cdot \mathbf{v} \, d\mathbf{x} = 0 \tag{1}$$

$$\int_{\Omega_f} r \nabla \cdot \mathbf{u} \, d\mathbf{x} = 0 \tag{2}$$

$$\int_{\Omega_s} \rho_s \frac{\partial^2 \mathbf{w}}{\partial t^2} \mathbf{v} \, d\mathbf{x} + \int_{\Omega_s} \lambda \nabla \cdot \mathbf{w} \nabla \cdot \mathbf{v} + \mu(D(\mathbf{w}) : D(\mathbf{v})) \, d\mathbf{x} - \int_{\Gamma_{sf}} \boldsymbol{\lambda}_2 \cdot \mathbf{v} \, d\mathbf{x} = 0 \tag{3}$$

$$\int_{\Gamma_{sf}} \left(\mathbf{u} - \frac{\partial \mathbf{w}}{\partial t} \right) \cdot \mathbf{s} \, d\mathbf{x} = 0 \tag{4}$$

for all $(\mathbf{v}, r, \mathbf{s}) \in \mathbf{H}^1_{\Gamma_d}(\Omega) \times L^2(\Omega_f) \times \mathbf{H}^{-1/2}(\Gamma_{sf})$, with Dirichlet boundary conditions over $\Gamma_d \subset \Gamma$ and zero Neumann boundary conditions over $\Gamma_f \cap (\Gamma \setminus \Gamma_d)$ and $\Gamma_s \cap (\Gamma \setminus \Gamma_d)$. The physical constants ρ_f and μ_f are the density and the viscosity of the fluid and $D_{ij}(\mathbf{u}) = (\partial u_i/\partial x_j + \partial u_j/\partial x_i)/2$ is the deformation tensor. Also, $\lambda = Ev/(1+v)(1-2v)$ and $\mu = E/1 + v$ with the density ρ_s, Young's modulus E and the Poisson ratio v for the solid material. $H^k_{\Gamma_s}(\Omega)$ is the Sobolev space of order k with vanishing functions over $\Gamma_s \subset \Gamma$ [1]. We denote $L^2(\Omega) = H^0(\Omega)$ and use bold face notation for vector-valued functions and spaces. In this coupled problem formulation, $\lambda_1 \in \mathbf{H}^{-1/2}(\Gamma_{sf})$ is a Lagrange multiplier that corresponds to the force exerted by the fluid region on the solid domain on Γ_{sf} and similarly $\lambda_2 \in \mathbf{H}^{-1/2}(\Gamma_{sf})$ corresponds to the force exerted by the solid region on the fluid domain on Γ_{sf}. Equation (4) represents the velocity/displacement continuity constraint on Γ_{sf}, while the force balance is given by

$$\langle \boldsymbol{\lambda}_1 - \boldsymbol{\lambda}_2, \mathbf{s} \rangle_{\Gamma_{sf}} = 0 \quad \forall \mathbf{s} \in \mathbf{H}^{1/2}(\Gamma_{sf}) \tag{5}$$

The direct numerical simulation of this highly non-linear system, governing even the most simplified fluid–structure interaction, depends on the convergence of iterative solvers which in turn relies on

DOI: 10.1002/fld

the characteristics of the coupled system. Domain decomposition techniques with non-matching grids have become increasingly popular in this regard for obtaining fast and accurate solutions of problems involving coupled processes [2]. In the last few years, domain decomposition methods have also been developed in conjunction with multigrid techniques, [3–5]. The purpose of this paper is to introduce a flexible algorithm that can be used to solve the coupled system over both the liquid and solid domains. A multilevel domain decomposition algorithm with non-matching grid is used for solving the equation system. The solver allows to discretize with fine level meshes the regions of interest and with coarser level meshes the other parts of the domain.

2. SYSTEM DISCRETIZATION

Let the discrete domain Ω_h be partitioned into m non-overlapping sub-domains $\{\Omega_\mathrm{h}^i\}_{i=1}^m$ such that each interface $\Gamma_\mathrm{h}^{ij} = \partial\Omega_\mathrm{h}^i \cap \partial\Omega_\mathrm{h}^j$ $(i \neq j)$ is non-empty. By starting at the multigrid coarse level $l = 0$, we introduce a finite element discretization over each subdomain Ω_h^i with characteristic mesh parameter h. Based on a simple element midpoint refinement, different multigrid level meshes can be constructed to reach the top finest multigrid level $l = n$ [6].

Let $\mathbf{X}_\mathrm{h}^l(\Omega_\mathrm{h}) \subset \mathbf{H}^1(\Omega_\mathrm{h})$, $S_\mathrm{h}^l(\Omega_\mathrm{h}) \subset L^2(\Omega_\mathrm{h})$ and $\mathbf{R}_\mathrm{h}^l(\Gamma_\mathrm{h}) = \mathbf{X}_\mathrm{h}^l|_{\Gamma_\mathrm{h}} \subset \mathbf{H}^{1/2}(\Gamma_\mathrm{h})$ be the approximation spaces. At each level mesh l we chose the families of finite element spaces to satisfy appropriate stability and approximation properties that will allow us to build a regular conforming approximation [1]. We indicate with $\mathbf{P}_\mathrm{h}^l(\Gamma) \subset \mathbf{H}^{-1/2}(\Gamma)$ the dual space of $\mathbf{R}_\mathrm{h}^l(\Gamma)$. Over each multigrid level we have constructed a standard finite element mesh with the same number of nodes on both sides of the element interfaces, but in every subdomain Ω_h^i the equation system (1)–(5) can be solved over a different level mesh generating a solution at different levels over different subdomains with different number of nodes on both sides of the element interface.

Let $\Omega_\mathrm{h}^{i,l}$ be the subdomain i where the solution will be computed at the multigrid level l. In the rest of the paper we denote with the apex i, l the solution over the corresponding subdomains, i.e. for the velocity $\mathbf{z}^{i,l}$, and with no apex the extended solution over Ω_h, i.e. $\mathbf{z}$ for the extended velocity. We will refer to $\mathbf{z}$ as the global velocity vector defined as $\mathbf{z} = \mathbf{u}$ over Ω_f, $\mathbf{z} = \dot{\mathbf{w}}$ over Ω_s and $\mathbf{z} = \dot{\mathbf{w}} = \mathbf{u}$ in Γ_sf. Note that $\mathbf{z}^{i,l}$ is computed over each $\Omega_\mathrm{h}^{i,l}$ at the corresponding level l, but the extended velocity $\mathbf{z}$ on the top level n is defined over all Ω_h in a standard and regular way. By using the multigrid interpolation operator $\mathscr{I}_l^n$ the extended velocity $\mathbf{z}$ is therefore defined by $\mathbf{z}(\mathbf{x}, t) = \mathscr{I}_l^n \mathbf{z}^{i,l}(\mathbf{x}, t)$, for all $\mathbf{x} \in \Omega_\mathrm{h}^i$. We can easily generalize the notations to all the other field variables.

In order to account for the changing nature of the fluid and solid subdomains, we wish to define a dynamic mesh for the space discretization. However, to avoid extreme distortion, we choose to move the mesh independently of the fluid velocity in the interior of Ω_f. Such a scheme, called arbitrary Lagrangian–Eulerian formulation, is commonly applied when studying fluid–structure interaction [7]. Inside the solid region each point is moving according to the time derivative of the displacement $\mathbf{w}$. In the fluid domain Ω_f, we define an independent grid velocity $\mathbf{u}_\mathrm{g}$ to be any smooth vector field satisfying the following boundary conditions $\mathbf{u}_\mathrm{g} = \partial\mathbf{w}/\partial t$ on Γ_sf and $\mathbf{u}_\mathrm{g} \cdot \hat{n} = 0$ on Γ_f. If the grid velocity is known as a function of time, the trajectory inside the domain Ω_f of a generic point of coordinate $\mathbf{x}(t)$ can be traced and its Lagrangian derivative of the new velocity field evaluated along the point trajectory. The Navier–Stokes equations in (1) can be considered in the Lagrangian form, taking into account that the fluid domain follows the characteristic line

DOI: 10.1002/fld

generated by the independent grid velocity $\mathbf{u}_g$, and the Lagrangian derivative can be discretized in time using a simple first-order integration scheme with time step Δt. In the rest of the paper we denote with $\mathbf{z}_t$ the explicit velocity evaluated at $(t, \mathbf{x}(t))$ and $\mathbf{z}_{t+\Delta t}$ the implicit velocity of the same point, now in $\mathbf{x}(t+\Delta t)$, evaluated in the new domain configuration $\Omega_f(t+\Delta t)$ and at the time $t+\Delta t$. With this notation the elasticity equation is discretized in time by a standard Newmark integration scheme and the velocity $\dot{\mathbf{w}}$, the acceleration $\ddot{\mathbf{w}}$ of the displacement $\mathbf{w}$ are introduced by standard first-order expansion [7, 8].

Following the above proposed numerical schemes, system (1)–(5) can be discretized in time and space. Let J^i be the set of the j-indices of all the neighboring regions Ω^j surrounding the subdomain Ω^i. Let $(\mathbf{z}^{i,l}, p^{i,l}, \boldsymbol{\tau}^{ij,l}) \in \mathbf{X}_h^l(\Omega^i) \times S_h^l(\Omega_f^i) \times \mathbf{P}_h^l(\Gamma^{ij})$ be the global velocity, the pressure and the stress vector, over the corresponding subdomains. The variable state $(\mathbf{z}^{i,l}, p^{i,l}, \boldsymbol{\tau}^{ij,l})$ satisfies the discrete system

$$\begin{aligned}
&\int_{\Omega_f} \rho_f \left(\frac{\mathbf{z}_{t+\Delta t}^{i,l}}{\Delta t} + ((\mathbf{z}_{t+\Delta t}^{i,l} - \mathbf{u}_g^{i,l}) \cdot \nabla) \mathbf{z}_{t+\Delta t}^{i,l} \right) \cdot \mathbf{v}^{i,l} \, d\mathbf{x} + \int_{\Omega_s} \rho_s a_1 \mathbf{z}_{t+\Delta t}^{i,l} \cdot \mathbf{v}^{i,l} \, d\mathbf{x} \\
&\quad + \int_{\Omega_f} (2\mu_f D(\mathbf{z}_{t+\Delta t}^{i,l}) : D(\mathbf{v}^{i,l}) - p_{t+\Delta t}^{i,l} \nabla \cdot \mathbf{v}^{i,l}) \, d\mathbf{x} + \int_{\Gamma_h^{ij}} \boldsymbol{\tau}^{ij,l} \cdot \mathbf{v}^{i,l} \, d\mathbf{x} \\
&\quad + \int_{\Omega_s} a_2 (\lambda \nabla \cdot \mathbf{z}_{t+\Delta t}^{i,l} \nabla \cdot \mathbf{v}^{i,l} + \mu D(\mathbf{z}_{t+\Delta t}^{i,l}) : D(\mathbf{v}^{i,l})) \, d\mathbf{x} \qquad (6) \\
&= \int_{\Omega_s} (\lambda \nabla \cdot (a_4 \dot{\mathbf{w}}_t^{i,l} - \mathbf{w}_t^{i,l} + a_5 \ddot{\mathbf{w}}_t^{i,l}) \nabla \cdot \mathbf{v}^{i,l} + \mu D(a_4 \dot{\mathbf{w}}_t^{i,l} + a_5 \ddot{\mathbf{w}}_t^{i,l} - \mathbf{w}_t^{i,l}) : D(\mathbf{v}^{i,l})) \, d\mathbf{x} \\
&\quad + \int_{\Omega_f} \rho_f \frac{\mathbf{u}_t^{i,l}}{\Delta t} \cdot \mathbf{v}^{i,l} \, d\mathbf{x} + \int_{\Omega_s} \rho_s (a_1 \dot{\mathbf{w}}_t^{i,l} + a_3 \ddot{\mathbf{w}}_t^{i,l}) \cdot \mathbf{v}^{i,l} \, d\mathbf{x} \quad \forall \mathbf{v}^{i,l} \in \mathbf{X}_h^l(\Omega^i)
\end{aligned}$$

$$\int_{\Omega_f} r_{t+\Delta t}^{i,l} \nabla \cdot \mathbf{z}_{t+\Delta t}^{i,l} \, d\mathbf{x} = 0 \quad \forall r^{i,l} \in S_h^l(\Omega_f^i) \qquad (7)$$

$$\int_{\Gamma_h^{ij}} (\mathbf{z}^{i,l} - \mathbf{z}^{j,k}) \cdot \mathbf{s}^{ij,l} \, d\mathbf{x} = 0 \quad \forall \mathbf{s}_f^{ij,l} \in \mathbf{P}_h^l(\Gamma_h^{ij}) \qquad (8)$$

for all $j \in J^i$ and $i = 1, 2, \ldots, m$. The appropriate exterior boundary conditions on Γ_f and Γ_s complete the formulation of problem (6)–(8). The coefficients $a_1 = 1/\alpha\Delta t$, $a_2 = \Delta t\gamma/2\alpha$, $a_3 = -\alpha - 1/\alpha$, $a_4 = -\Delta t(1 - \gamma/2\alpha)$, $a_5 = -\Delta t^2/2(1 - \gamma/\alpha)$ are obtained from the standard Newmark integration scheme of the first order [7, 8]. All the terms on the right-hand side of (6), w_t, $\dot{w}_t$ and $\ddot{w}_t$, are evaluated in the previous time step. Once Equation (1) is solved for $\dot{\mathbf{z}}_{t+\Delta t}$, $p^{i,l}$ and $\boldsymbol{\tau}^{ij,l}$, the displacement $\mathbf{w}_{t+\Delta t}$ and its acceleration $\ddot{\mathbf{w}}_{t+\Delta t}$ can be computed by using the standard Newmark expansions. On the shared boundaries Γ_h^{ij} the stress vectors, $\boldsymbol{\tau}^{ij,l}$ and $\boldsymbol{\tau}^{ji,k}$, belong to the two different spaces $\mathbf{P}_h^l$ and $\mathbf{P}_h^k$. The stress vectors are the same in weak sense and can be computed easily among the different level meshes since the boundary vector spaces are nested, with $\mathbf{R}_h^l \subseteq \mathbf{R}_h^k$ $(l \leqslant k)$. It is worth noticing that the constraints on the fluid–structure interface are implicitly satisfied

DOI: 10.1002/fld

by Equation (6). No extra equations are necessary in order to ensure the velocity/displacement continuity and force balance on the common interface.

The entire system is solved using a fully coupled iterative multigrid solver with a Vanka-type smoother [6, 9]. Multigrid solvers for coupled velocity/pressure system compute simultaneously the solution for both the pressure and the velocity field, and they are known to be one of the best class of solvers for laminar Navier–Stokes equations and more in general for elliptic problems (see [9]). An iterative coupled solution for the linearized discretized system requires the solution of a large number of sparse problems. In order to optimally solve the equation system (6)–(8), involving the unknown stress vector $\boldsymbol{\tau}^{ij}$, we use this block Gauss–Seidel method, where each block consists of a small number of degrees of freedom. The characteristic feature of this type of smoother is that in each smoothing step a large number of small linear systems of equations have to be solved. Each block of equations corresponds to all the degrees of freedom that are connected to few elements.

3. NUMERICAL TESTS

In this section we test the fluid–structure non-conforming formulation [10]. As shown in Figure 1 on the left, let the rectangular region $\Omega = [0.02\,\mathrm{m}] \times [0.01\,\mathrm{m}]$ be the computational domain with boundary Γ. The solid region Ω_s consists of a beam, clamped at the point $(0.005\,\mathrm{m}, 0)$, with length equal to 0.006 m and thickness equal to 0.0005 m. The head of the beam has been smoothed with a semicircle centered in 0.005, 0.00575 m and radius $r = 0.00025\,\mathrm{m}$. The fluid and the solid boundaries, Γ_f and Γ_s, are the contours of the two shaded regions and their intersection is labeled by Γ_{sf}. On the right and left sides, the channel outflow and inflow boundary conditions, with parabolic profile ($\max\ \mathrm{vel} = 0.05\,\mathrm{m/s}$), are considered. The initial conditions for the velocity field are set to zero.

The fluid and the solid properties are chosen in order to produce large deformations of the beam and to test the reliability of the solver in challenging situations. The fluid density ρ_f and viscosity μ_f are equal to $1000\,\mathrm{kg/m^3}$ and $0.001\,\mathrm{kg/m\,s}$, respectively. The solid density ρ_s, Young's module E and the Poisson ratio v are $1000\,\mathrm{kg/m^3}$, 50 000 Pa and 0.48, respectively.

The time step $\Delta T = 0.001\,\mathrm{s}$ has been used for a total of 1000 time steps (1 s). Only the four level meshes, l_0, l_1, l_2 and l_3, are considered. The number of unknowns (global velocity field and pressure) involved in the computation at the mesh level l_3 is quite large, approximatively 70 000. By using different levels over different subregions more efficient computations can be obtained. As shown in Figure 1 on the right, the domain Ω is split into two subdomains Ω^1, Ω^2, and two different non-conforming meshes are built. In the subdomain Ω^1 the mesh level l_3 is always used. In order to reduce the solution unknowns over Ω^2 low mesh levels are considered. We label with P_1, P_2 the case where the levels l_2, l_1 are used. Approximatively 45 000 and 40 000 are the new numbers of unknowns for the new configurations P_1 and P_2. The computational CPU time and the allocation memory expenses are proportionally reduced. In Figure 2 (on the left), the non-conforming case P_2 with the levels l_3 and l_1 is reported over the domain decomposition Ω_1 and Ω_2. In Figure 2 on the right, the beam extrema oscillation is compared for the three conforming meshes l_3, l_2 and l_1, and for the two non-conforming meshes P_1 and P_2. The results show clear advantages of the non-conforming discretizations over the conforming ones. Obviously, the path obtained with the finest mesh l_3 can be considered the most accurate. The l_1 path is mostly below the l_3, showing too much stiffness in the beam response. The beam oscillation obtained with the non-conforming

DOI: 10.1002/fld

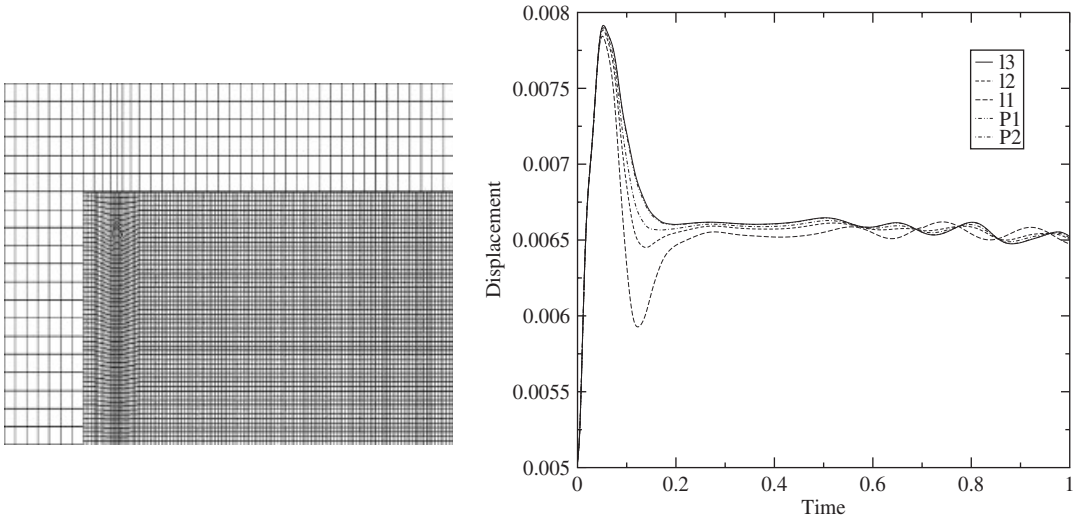

Figure 2. Non-conforming mesh configurations P_2 (left) and beam extrema oscillations.

configuration P_1 almost overlaps the result obtained with the conforming mesh l_3. There are very small differences between the path in l_3 and the path in P_2. These results clearly indicate how one can use the non-conforming multilevel partitioning to preserve the same accuracy in regions of interest. It should be noticed that the comparisons have been tested on a beam displacement oscillation, which is indirectly related to the multilevel domain partitioning. The sensitivity of the beam response to the different level meshes and the different domain decompositions points out again to the fact that the system is fully coupled.

4. CONCLUSION

New discretizations both in time and space have been presented for the coupled non-linear FSI problem. In particular it is possible to rewrite and solve the coupled system for both the fluid and structure equations in terms of the global velocity and pressure. A non-conforming multilevel finite element method discretization embedded in a geometric multigrid algorithm has been used together with a Vanka smoother in order to solve the coupled system. Preliminary results indicate the stability of the algorithm and show that the use of the non-conforming multilevel partitioning preserves the same accuracy in regions of interest, reducing at the same time the computational CPU time and memory allocation.

REFERENCES

1. Girault V, Raviart P. *The FEM for Navier–Stokes Equations*: *Theory and Algorithms*. Springer: New York, NY, 1986.
2. Bernardi C, Maday Y, Patera AT. Domain decomposition by the mortar element method. In *Asymptotic and Numerical Methods for Partial Differential Equations with Critical Parameters*, Kaper H *et al.* (eds). Reidel: Dordrecht, 1993; 269–286.

DOI: 10.1002/fld

3. Aulisa E, Manservisi S, Seshaiyer P. A computational multilevel approach for solving 2D Navier–Stokes equations over non-matching grids. *Journal of Applied Mechanics and Engineering* 2006; **195**:4604–4616.
4. Aulisa E, Manservisi S, Seshaiyer P. A non-conforming computational methodology for modeling coupled problems. *Nonlinear Analysis* 2005; **63**:1445–1454.
5. Braess D, Dahmen W, Wieners C. A multigrid algorithm for the mortar finite element method. *SIAM Journal on Numerical Analysis* 1999; **37**(1):48–69.
6. Manservisi S. Numerical analysis of Vanka-type solvers for steady Stokes and Navier–Stokes flows. *SIAM Journal on Numerical Analysis* 2006; **44**/**5**:2025–2056.
7. Donea J, Giuliani S, Halleux J. An arbitrary Lagrangian Eulerian finite element method for transient fluid–structure interactions. *Computer Methods in Applied Mechanics and Engineering* 1982; **33**:689–723.
8. Reddy JN. *An Introduction to the Finite Element Method* (2nd edn). McGraw-Hill: New York, 1993.
9. John V, Tobiska L. Numerical performance of smoothers in coupled multigrid methods for the parallel solution of incompressible Navier–Stokes equations. *International Journal for Numerical Methods in Fluids* 2000; **33**:453–473.
10. Turek S, Hron J. Proposal for the numerical FSI benchmarks. *Report*, University of Dortmund, 2005.

DOI: 10.1002/fld